THE ASTROPHYSICAL JOURNAL, 363:131–141, 1990 November 1

GINGA OBSERVATIONS OF X-RAYS FROM THE SEYFERT I GALAXY MARKARIAN 509

K. P. SINGH
Tata Institute of Fundamental Research, Bombay
N. J. WESTERGAARD AND H. W. SCHNOPPER
Danish Space Research Institute, Lyngby, Denmark
AND
H. AWAKI AND Y. TAWARA
Department of Astrophysics, Nagoya University
Received 1989 December 11; accepted 1990 April 30

ABSTRACT

We present the X-ray light curves and X-ray spectra of Markarian (Mrk) 509 from two observations with the *Ginga* satellite. A continuously varying X-ray intensity on hourly time scales was observed on both the occasions. The observed variability is the fastest reported so far from Mrk 509. The X-ray intensity was observed to increase almost linearly before saturating at the maximum on 1988 October 8 and thus showing a quadratic trend. About 5 days later it was observed to decrease linearly. The maximum variation observed is 30%. The X-ray spectra accumulated for different intensity levels were analyzed separately. We find that the 1–30 keV spectra are best explained by (*a*) a variable power law with the photon index Γ in the range of 1.6–1.7 over the energy bandwidth of 3–30 keV and showing a steepening with increase in the intensity, (*b*) a variable low-energy excess below 3 keV with a very steep spectrum ($\Gamma = 4.5 \pm 1.0$ or a blackbody with $kT \simeq 0.3$ keV or an accretion disk with $kT \simeq 0.4$ keV), (*c*) a Gaussian line feature near 6 keV best observed during the peak brightness level and having an equivalent width of 150 ± 49 eV, and (*d*) good evidence for a flatter ($\Gamma \simeq 1.47 \pm 0.07$) spectrum above 10 keV during the maximum brightness. The observations are consistent with the presence of a large amount of cold matter around the dominant nonthermal X-ray source in the active galactic nucleus of Mrk 509 even though no low-energy absorption is observed directly.

Subject headings: galaxies: individual (Markarian 509) — galaxies: nuclei — galaxies: Seyfert — galaxies: X-rays — radiation mechanisms — spectrophotometry

I. INTRODUCTION

The nuclei of Seyfert galaxies are well known to be prolific emitters of X-rays. One of the nearest ($z = 0.0355$) and among the brightest such objects is Markarian 509 (Mrk 509) classified as a Seyfert type I galaxy. Its compact optical appearance and luminosity bear a close resemblance to that of a QSO (Kopylov *et al.* 1974). It is also a weak radio source (Ulvestad and Wilson 1984; Antonucci and Barvainis 1988). It was first identified as an X-ray source by Cooke *et al.* (1978) based on the observations made with the *Ariel V* satellite. The identification was confirmed by Dower *et al.* (1980) using the scanning modulation collimator onboard the *HEAO 1* satellite. Subsequent X-ray observations over an energy range of 0.1–165 keV have been carried out with a number of experiments (Mushotzky *et al.* 1980; Dil *et al.* 1981; Rothschild *et al.* 1983; Petre *et al.* 1984; Singh, Garmire, and Nousek 1985; and Morini, Lipani, and Molteni 1987). The 2–100 keV X-ray spectrum of Mrk 509 as measured in 1978 October is a power law with a photon index $\Gamma = 1.64 \pm 0.04$ (Rothschild *et al.* 1983). The 0.75–4.5 keV and 1–10 keV spectral measurements in 1979 April–May with the *Einstein Observatory* indicated a value of Γ closer to 1.9 (Petre *et al.* 1984). An excess low-energy spectral component dominating below 1 keV was first detected by Singh Garmire, and Nousek (1985) and later confirmed by Morini, Lipani, and Molteni (1987), making it the first Seyfert galaxy for which such an excess has been confirmed with two independent experiments. Similar soft X-ray excesses have been seen in many Seyferts (Turner and Pounds 1989) and confirmed in a few cases like NGC 4151 (Warwick *et al.* 1989). The ultraviolet to the optical (1200 Å–10 μm) continuum of Mrk 509 has a significantly steeper power law spectrum (Wu, Boggess, and Gull 1983; Philips *et al.* 1983 and references therein) but consistent with the existence of the soft X-ray excess. The optical emission from its nucleus is variable. Both the optical continuum and the optical line emission have been found to change. The 2–10 keV intensity of Mrk 509 is also erratic (Petre *et al.* 1984), and a nearly 25% increase has been seen on a time scale of 12 days from the *EXOSAT* (*European X-Ray Astronomy Satellite*) observations (Morini, Lipani, and Molteni 1987). An increase in its soft X-ray emission unrelated to the variation in the harder X-rays is also evident from the *EXOSAT* observations. A careful reanalysis of the *EXOSAT* spectral data using the information from only the most reliable detectors (see Singh *et al.* 1989) shows that its photon spectra can be characterized by a single power law ($\Gamma = 1.9 \pm 0.07$) for energies in the range of 1–10 keV and a steeper component below 1 keV which can be modeled by either a power law ($\Gamma \simeq 4$) or a blackbody ($kT \simeq 0.07$ keV). A line feature near 6 keV has also been previously reported by Morini, Lipani, and Molteni (1987) from their analysis.

We present here the high-sensitivity X-ray observations of Mrk 509 performed with the Japanese X-ray astronomy satellite *Ginga*. A preliminary report was presented earlier by Singh *et al.* (1989). A detailed analysis of the X-ray intensity variations and the X-ray spectrum is presented. The paper is organized as follows. In § II we present the details of the observations followed by the analysis and the results obtained in § III. In § IV we discuss the results.

II. OBSERVATIONS

The observations were made in 1988 October with the Large Area Proportional Counters (LAC) onboard the Japanese X-ray astronomy satellite *Ginga* as a part of their Guest Investigator program. The total effective area of the LAC is 4000 cm^2 (Turner *et al.* 1989), where the detection efficiency over an energy range of 1–37 keV has been included. The detector field of view (fov) is 1° × 2° (FWHM). The details of the *Ginga* and the LAC are given by Makino (1987) and Turner *et al.* (1989). The LAC was pointed at Mrk 509 on 1988 October 8 from 0 to 14 UT and again from 21 UT on October 12 to 10.5 UT on 1988 October 13, and data were obtained in the MPC1 mode (see Makino 1987) with a time resolution of 16 s. There is no other cataloged X-ray source in the fov of the LAC. The background measurements were made from a source-free region centered at a position about 3° north of Mrk 509 and data accumulated from 06 to 11 UT on October 9 and from 00 to 17 UT on 1988 October 12. The behavior of the background in the LAC and the procedure for the data selection and the background subtraction are described in detail by Hayashida *et al.* (1989). According to the criterion described by Hayashida *et al.*, useful data from the source-free region as well as the Mrk 509 observation were accumulated separately for the "contact" and the "remote" orbits (with respect to the South Atlantic Anomaly, SAA) for the following periods with (*a*) low charged particle background, (*b*) the satellite positions where the rigidity cut off is greater than 10 GeV, and (*c*) the Earth elevation angle greater than 7°.

The position of the Sun was "behind" the LAC during our observations; therefore, solar contamination is not expected. The total useful exposure on the source thus realized is about 6.5 hr. The log of observations and useful exposure times obtained is in Table 1. The background-subtracted source count rates are also listed in Table 1. The observations are divided into a number of files for detailed spectral fitting (see § III*b*).

III. ANALYSIS AND RESULTS

a) X-Ray Light Curves

The total count rates in the selected LAC data (see § II) include contributions from the X-ray background, charge particle–induced background, and weak and variable radioactive features induced while transiting through the SAA, apart from the X-ray source in the field of view, as described in Hayashida *et al.* (1989). These contributions to the background are very well modeled using the blank sky (i.e., free of any known X-ray sources) data, by performing a multiparameter least-squares fit to the count rates in each spectral channel. For this purpose the blank sky data are obtained as close as possible to the source observation and the background parameters obtained are used to model the background during the source observation. This is currently the standard procedure for the reduction of the *Ginga* data and is described by Hayashida *et al.* (1989). We took extra care by modeling the "contact" (with respect to SAA) and "remote" orbits data separately to reduce the systematics even further. We also verified our results by using the background models obtained from a large number of accumulated blank field data, and also by interchanging the two backgrounds obtained a few days apart for this observation. We estimate that the residual effect of improper background subtraction is no more than 5% of the total counts attributed to the X-rays from Mrk 509, in a 128 s integration. The background-subtracted data were then summed into different energy channels, formed from the pulse height (PH) channels, viz., (1) 1.2–2.3 keV, (2) 2.3–9.9 keV, and (3) 9.9–18.7 keV, hitherto referred to as channel 1, channel 2, and channel 3, respectively. The light curves thus produced were compared with the light curves obtained using method II of Hayashida *et al.* which uses background accumulated from a large number of background data sets, and the results were found to be almost identical. The background-subtracted X-ray count rate observed from Mrk 509 and integrated for every 256 s are displayed in Figure 1*a* for 1988 October 8 and in Figure 1*b* for 1988 October 12–13. Also shown in these figures is the hardness ratio defined as the ratio of the count rates in energy channel 2 divided by the count rates in the energy channel 1. The times when the satellite was in "contact" with the SAA and "remote" from it are marked in Figure 1. The X-ray intensity in channels 1 and 2 is seen to be changing. The X-ray light curves in Figure 1 were analyzed for finding the trend of variability. Both linear and quadratic expressions of the type $r = A + Bt$ and $r = A + Bt + Ct^2$, respectively, where r is the count rate and t is the time, were tried for modeling the observed variability. The results of this analysis are shown in Table 2. It is observed that for the data of 1988 October 8 the count rates in all the energy channels are best described by a quadratic trend where the intensity levels off after a few hours whereas on October 12–13 the count rates in the same energy channels are well fitted by a linearly decreasing trend except for a couple of points in channels 1 and 3 which appear more erratic and give a poor χ^2 for simple linear models. Using a quadratic expression for modeling the count rates of October 12–13 observation made no improvement to the fit. The parameters of the best-fit models are given in Table 2.

TABLE 1

OBSERVATION TIMES CORRESPONDING TO THE SPECTRAL FILES USED IN THE ANALYSIS

FILE NAME	STARTING TIME			ENDING TIME			EFFECTIVE EXPOSURE TIME (s)	SOURCE COUNT RATE[a] (1–30 keV)
	Day (1988 Oct)	Hour	Minute	Day (1988 Oct)	Hour	Minute		
S1	8	00	0	8	02	17	1742.5	24.4
S2	8	02	56.7	8	04	53.8	2335.8	28.0
S31.....	8	06	08.5	8	09	29.0	4330.8	30.0
S32.....	8	09	29.0	8	14	14.8	4278.2	31.0
S4	12	20	51.1	13	03	24.2	3860.6	27.0
S5	13	03	45.5	13	10	35.1	6765.8	24.0

[a] In the top layer of the LAC. Hours and minutes are UT.

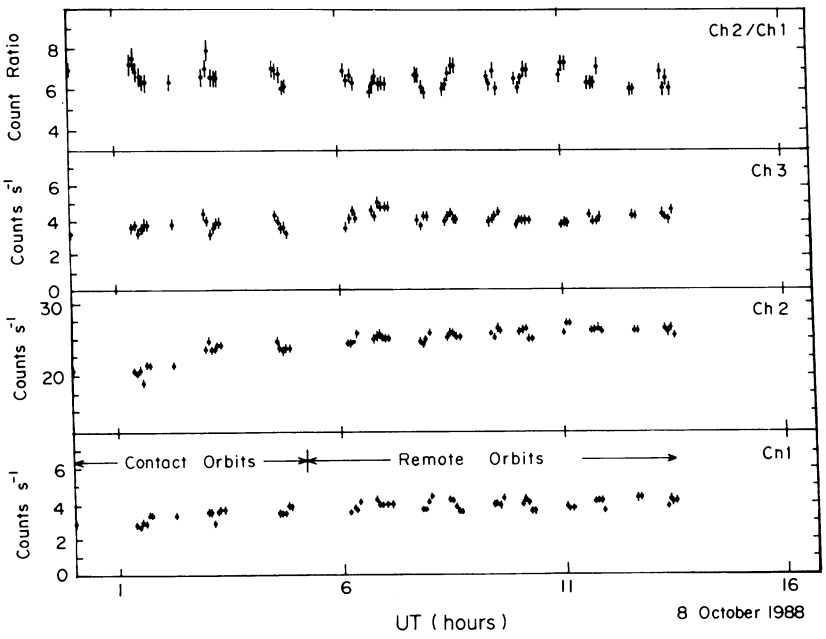

FIG. 1*a*

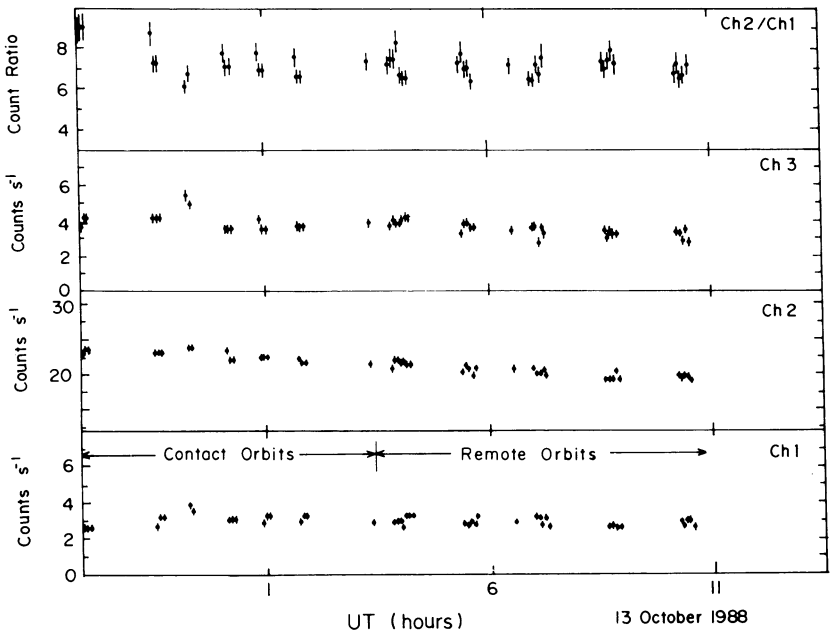

FIG. 1*b*

FIG. 1.—(*a*) The count rates in three energy ranges (channel 1: 1.2–2.3 keV; channel 2: 2.3–9.9 keV; channel 3: 9.9–18.7 keV) and the count ratio (channel 2/channel 1) observed with *Ginga* on 1988 October 8. (*b*) Same as in (*a*) for observations on 1988 October 12–13.

The variations in the channel 1 rates are well correlated with the variations in the channel 2 rates as shown in the correlation plot of Figure 2. The linear correlation coefficient (R) for the entire plot is 0.83 with the probability of its being exceeded in a random population being 6.9×10^{-29}. In this figure we show the data from the two observations separately (plus signs for the October 8 data and open circles for the October 12–13 data), and find that the high degree of correlation results mostly from the October 8 data which gives a value of 0.75 for R. The R for second set of data is only 0.41.

A correlation plot between the hardness ratio (HR1) defined as the ratio of counts in channel 2 to channel 1 and the counts in channel 1 is shown in Figure 3, where the data from the two observations are shown separately as in Figure 2. The plot depicts the complex nature of the observed variability in the source. A significant inverse linear correlation (R values as above for Fig. 2) between the hardness ratio and the low energy intensity is observed. The observed inverse correlation strongly suggests spectral variability of the continuum. The plot indicates a steepening of the underlying power-law continuum as

TABLE 2

RESULTS OF THE ANALYSIS OF THE OBSERVED COUNT RATES

Energy Band (keV)	Model	Best-Fit Parameters	χ_r^2 [a]	DOF[a]
		A. 1988 Oct 8 Observation		
1.2–2.3	Constant	A = 3.73 ± 0.03	4.42	59
	Linear	A = 3.13 ± 0.06	1.94	58
		B[b] = 2.36 ± 0.19		
	Quadratic	A = 2.82 ± 0.09	1.60	57
		B[b] = 5.80 ± 0.76		
		C[c] = −6.92 ± 1.5		
2.3–9.9	Constant	A = 24.6 ± 0.06	14.4	59
	Linear	A = 21.4 ± 0.14	3.7	58
		B[b] = 12.2 ± 0.50		
	Quadratic	A = 19.7 ± 0.22	2.1	57
		B[b] = 30. ± 2.		
		C[c] = −36. ± 3.8		
9.9–18.6.....	Constant	A = 4.0 ± 0.04	2.2	59
	Linear	A = 3.65 ± 0.08	1.7	58
		B[b] = 1.38 ± 0.25		
	Quadratic	A = 3.33 ± 0.12	1.5	57
		B[b] = 4.9 ± 1.		
		C[c] = −6.9 ± 2.		
		B. 1988 Oct 12–13 Observation		
1.2–2.3	Constant	A = 2.95 ± 0.03	2.6	45
	Linear	A = 3.57 ± 0.18	2.4	44
		B[b] = −6.13 ± 1.7		
2.3–9.9	Constant	A = 21.2 ± 0.07	9.2	45
	Linear	A = 30.5 ± 0.49	1.1	44
		B[b] = −9.15 ± 0.48		
9.9–18.6.....	Constant	A = 3.64 ± 0.04	3.8	45
	Linear	A = 5.89 ± 0.27	2.2	44
		B[b] = −2.21 ± 0.26		

[a] χ_r^2 is per degree of freedom, and DOF is the number of degrees of freedom.
[b] In units of 10^{-5} counts s^{-2}.
[c] In units of 10^{-10} counts s^{-3}.

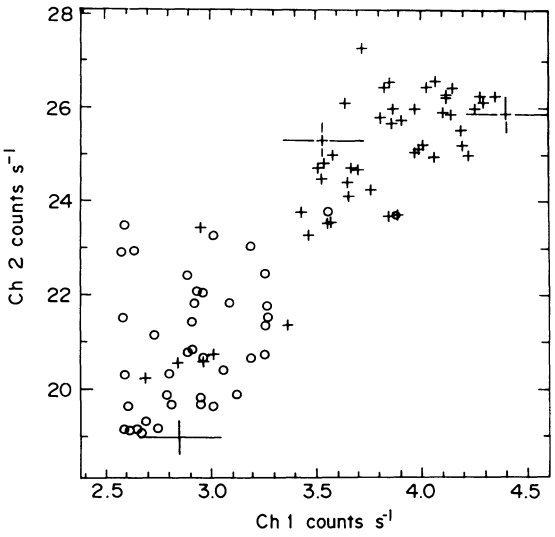

FIG. 2.—The correlation between the count rates in the 1.2–2.3 keV vs. the count rates in the 2.3–9.9 keV energy bands. The data from the October 8 observations are shown with plus signs, and the data from the October 12–13 are shown with the open circles.

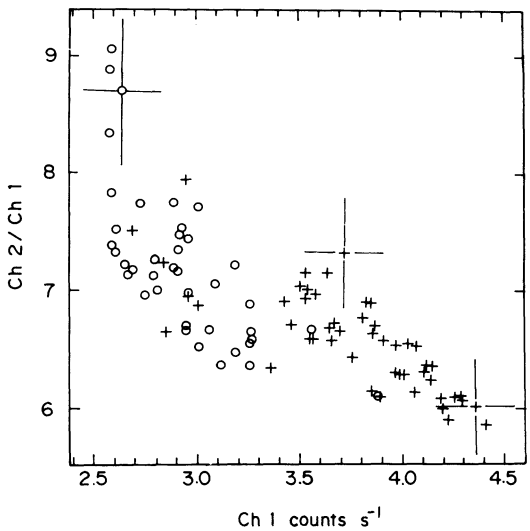

FIG. 3.—The correlation plot of the hardness ratio as defined in the text and the count rates in channel 1. The symbols are as in Fig. 2.

the source intensity increases. This motivated us to investigate the spectral variations by a detailed fitting of the spectral data collected at different intensity levels of the source.

b) X-Ray Spectrum

The pulse height spectra over an energy range of 1–30 keV were accumulated for the different intensity levels of the X-ray source. After studying the ratio of the counts in the top layer to the midlayer of the LAC, six PH spectra (see Table 1) were created using only the top layers of the LAC which detected about 90% of the total photons. The top layer data also has the best signal-to-noise ratio, as most of the source counts above background are in the 2–10 keV range and where the midlayer has lower effective area but background comparable to that in the top layer. This scheme also had the merit of treating the "contact" and "remote" orbits data separately. These data sets will henceforth be referred to as S1, S2, S31, S32, S4, and S5, where the first four are from the observations made on 1988 October 8 and the rest from the 1988 October 12–13. The time spans for these data sets are given in Table 1. These data sets were analyzed individually to study the spectral variations. A systematic error of 1% was assumed for the counts in each PH channel. The following spectral analyses were then carried out by using the detector response function.

We assume throughout that the equivalent hydrogen column density N_H due to the interstellar medium in the line of sight to Mrk 509 is 4×10^{20} cm^{-2}, close to that given by the 21 cm measurements (Heiles, 1975). The abundances and the cross sections for the absorbing column are from Morrison and McCammon (1983). We first tried a simple power-law model and found it inadequate to explain any of the observed 1–30 keV spectra. Such a model is rejected by the χ^2 statistic. As an example, the X-ray spectrum corresponding to the data set S32 obtained on 1988 October 8 when the source was at its brightest is displayed in Figure 4*a*. The best-fit single power-law model to the data is shown as a histogram. The poor quality of the fit is evident from the large residuals around 3 and 6 keV. Figure 5*a* which displays the S5 data set obtained during the minimum observed brightness level shows a similar effect as in Figure 4*a* for a simple power law. The 3–30 keV spectra were analyzed next. For the 3–30 keV data a single power-law continuum is found to give an acceptable χ^2 for the S1 and S2 spectra. The inclusion of a Gaussian-like emission line (with a fixed width of 50 eV) near 6 keV leads to a further improvement in the fits for all the spectra except the S4. It is, however, necessarily required to explain the S32 and S5 spectra.

There is a remarkable improvement in the χ^2 when an additional model for the excess low-energy component (mainly below 3 keV) is included in the fitting procedure for the 1–30 keV data. Three different models were separately tried for fitting the low-energy continuum. These are (*a*) a power law, (*b*) a black body spectrum, and (*c*) an accretion disk spectrum (Makishima *et al.* 1986). The photon index obtained from the best-fit power law (and a Gaussian line wherever necessary) to the 3–30 keV data was fixed while fitting the 1–30 keV data with two continuum spectral models and a Gaussian line. The fact that the addition of a steep soft component and a Gaussian line feature near 6.5 keV is necessary for obtaining a good fit to the data is shown in the Figures 4*b* and 5*b*. The individual

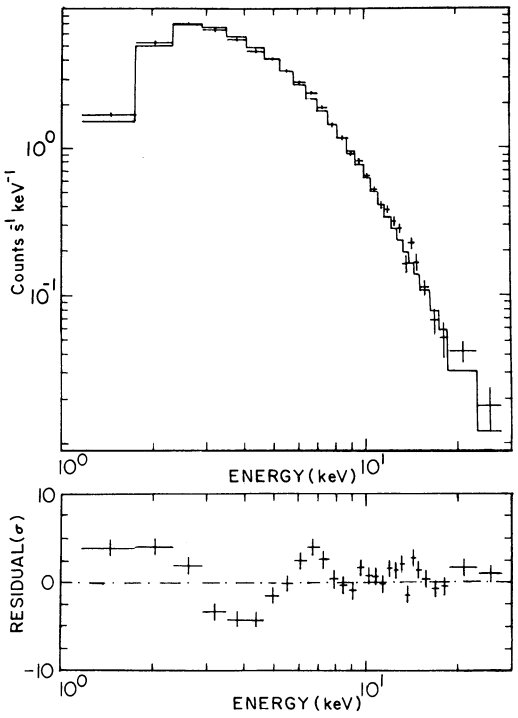

FIG. 4*a*

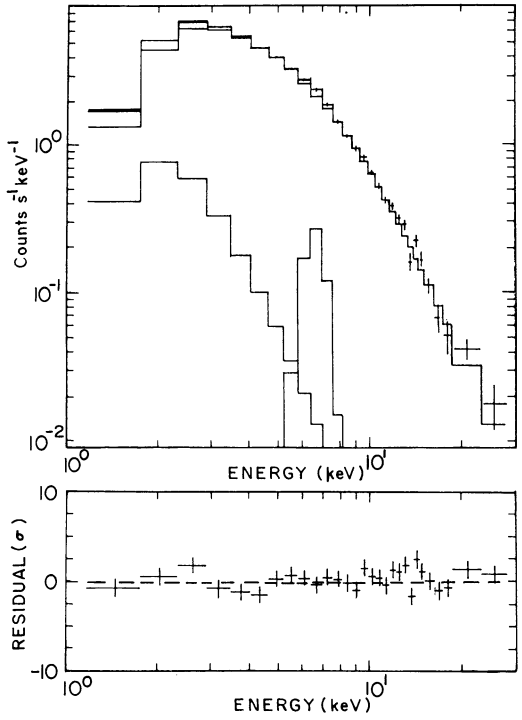

FIG. 4*b*

FIG. 4.—(*a*) The 1–30 keV PH spectrum as observed with *Ginga* on 1988 October 8 during the maximum brightness and the best-fit single power-law model shown as a histogram. The inadequacy of the simple model to explain the data is evident from the residuals. (*b*) The data are the same as in (*a*), but the best-fit model now contains two continuum components (both power laws) and a Gaussian feature near 6 keV and gives an acceptable fit to the PH data. The contributions of all the components of the model are shown separately as histograms.

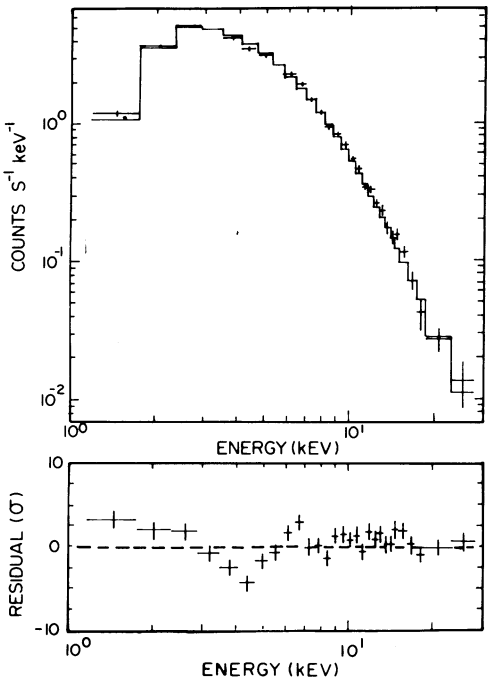

FIG. 5*a*

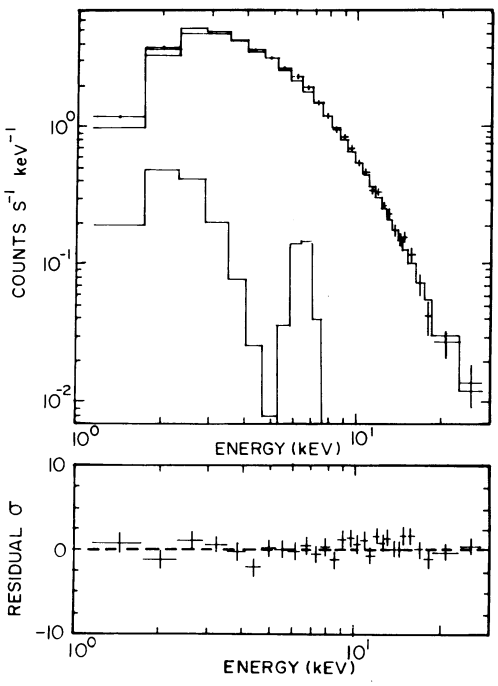

FIG. 5*b*

FIG. 5.—(*a*) The 1–30 keV PH spectra as observed with *Ginga* on 1988 October 13 during the minimum brightness and the best-fit single power-law model shown as a histogram. The inadequacy of the simple model to explain the data is evident from the residuals. (*b*) The data are the same as in (*a*), but the best-fit model now contains two continuum components (power law and a blackbody) and a Gaussian feature near 6 keV and gives an acceptable fit to the PH data. The contributions of all the components of the model are shown separately as histograms.

contributions of all components are displayed here. The low-energy component shown in Figure 4*b* is a power law, and that shown in Figure 5*b* is a blackbody spectrum.

A summary of the results obtained from our spectral analysis is presented in Tables 3A and 3B. The best-fit model parameters and their associated 90% errors are listed in Table 3 for all the spectral data sets. We find, using the *F*-statistic, that the low-energy excess is better fitted with a blackbody ($kT = 0.3$ keV) or an accretion disk ($kT = 0.4$ keV) spectrum than a steep power law ($\Gamma = 4.5$). The relative contribution of the blackbody component to the 1–3 keV flux ranges from 18% to 20% for the October 8 data to 14% for the October 12–13 data. The blackbody component thus does not appear to vary proportionately to the power-law component.

The X-ray flux values and the equivalent widths estimated from the above analysis are listed in Table 4. The equivalent width of the line best observed during the peak brightness level is 150 ± 49 keV. For a comparison, we also list the X-ray flux values observed in 1983 with the *EXOSAT* (Singh *et al.* 1989).

c) X-Ray Spectral Variability

It was pointed out in § III*a* that the observed inverse correlation in Figure 3 could arise due to the steepening of the dominant power law continuum as the source intensity increases. We can investigate this further based on the detailed spectral analysis presented above. The best estimates of the power-law indices obtained from the acceptable two-component fit to the 3–30 keV spectral data at different times (see Table 3) are shown plotted against the observed X-ray intensity (I_x) of the source in Figure 6. The error bars indicated for Γ are at the 90% confidence level. There is marginal evidence for a steepening of the power law continuum as the source intensity increases. The linear correlation coefficient for the Γ versus I_x is 0.64 which corresponds to a probability of 16% for its being exceeded in a random population. The hypothesis of a constant average value 1.65 for the Γ, however, gives a reduced χ^2 of 3.7 signifying that Γ is indeed variable.

The same effect is shown in a model independent way in Figure 7, which is a plot of the ratio of counts in all the PH bins for the brightest phase (06 to 14 UT on October 8) to the corresponding counts while in the lowest intensity state observed on both October 8 and 13 (i.e., S1 + S5). The ratio is not a constant. The reduced χ^2 is 2.25 for 23 degrees of freedom corresponding to a probability of 5.5×10^{-4} for exceeding the

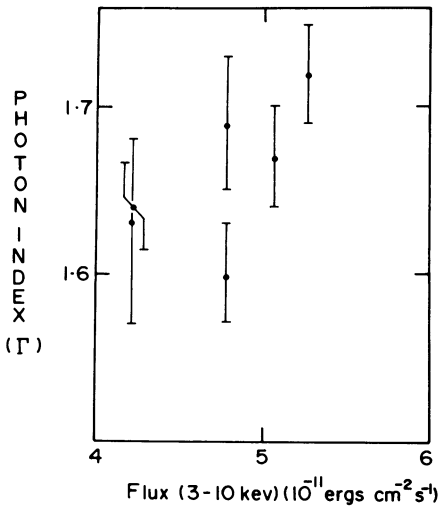

FIG. 6.—The power-law index Γ obtained from the best fits to the X-ray spectra vs the X-ray intensity. The plotted error bars are with 90% confidence.

TABLE 3

RESULTS OF MODEL FITTING TO THE X-RAY SPECTRA OF MRK 509

Serial Number	Energy Range[a]	Model[b]	A_1[c]	Γ_1	A_L[c]	E_L[a]	Γ_2	kT[a]	χ_r^2[d]	DOF[d]
A. 1988 Oct 8: *Ginga* LAC Observations										
Spectral File S1 (Minimun Intensity)										
1.....	3–30	PL	45.0 ± 3.4	1.61 ± 0.05	...	...	...	...	1.25	24
2.....	3–30	PL + line	45.7 ± 3.6	1.63 ± 0.05	0.18 ± 0.2	6.45 ± 0.65	...	...	1.27	22
3.....	1–30	PL	53.8 ± 2.3	1.71 ± 0.03	...	...	...	...	2.10	27
4.....	1–30	PL + line	54.8 ± 2.7	1.73 ± 0.04	0.25 ± 0.2	6.50 ± 0.5	...	...	2.10	25
5.....	1–30	PL + PL + line	45.0 ± 1.3	1.63	0.25 ± 0.2	6.45 ± 0.5	4.60 ± 1.35	...	1.21	24
6.....	1–30	PL + line + BB	45.5 ± 1.1	1.63	0.23 ± 0.2	6.43 ± 0.5	...	0.32 ± 0.08	1.13	24
7.....	1–30	PL + line + AD	45.4 ± 1.2	1.63	0.23 ± 0.2	6.43 ± 0.5	...	0.40 ± 0.10	1.14	24
Spectral File S2										
1.....	3–30	PL	57.5 ± 3.5	1.68 ± 0.04	...	...	...	...	0.98	24
2.....	3–30	PL + line	58.0 ± 3.7	1.69 ± 0.05	0.17 ± 0.18	6.14 ± 0.6	...	...	0.97	22
3.....	1–30	PL	66.4 ± 2.5	1.76 ± 0.03	...	...	...	...	1.88	27
4.....	1–30	PL + line	67.2 ± 2.6	1.78 ± 0.03	0.21 ± 0.18	6.17 ± 0.5	...	...	1.90	25
5.....	1–30	PL + PL + line	56.8 ± 1.7	1.69	0.22 ± 0.19	6.13 ± 0.5	4.65 ± 1.30	...	0.92	24
6.....	1–30	PL + line + BB	57.4 ± 1.2	1.69	0.21 ± 0.19	6.11 ± 0.5	...	0.30 ± 0.07	0.84	24
7.....	1–30	PL + line + AD	57.3 ± 1.2	1.69	0.22 ± 0.19	6.10 ± 0.5	...	0.40 ± 0.10	0.85	24
Spectral File S31										
1.....	3–30	PL	59.2 ± 2.6	1.66 ± 0.03	...	...	...	...	1.60	24
2.....	3–30	PL + line	59.5 ± 2.7	1.67 ± 0.03	0.19 ± 0.13	6.1 ± 0.4	...	...	1.50	22
3.....	1–30	PL	70.3 ± 1.9	1.76 ± 0.02	...	...	...	...	4.00	27
4.....	1–30	PL + line	71.0 ± 2.0	1.77 ± 0.02	0.21 ± 0.13	6.3 ± 0.4	...	...	4.00	25
5.....	1–30	PL + PL + line	58.0 ± 1.3	1.67	0.25 ± 0.14	6.1 ± 0.3	4.4 ± 0.75	...	1.55	24
6.....	1–30	PL + line + BB	58.6 ± 0.9	1.67	0.25 ± 0.14	6.1 ± 0.3	...	0.34 ± 0.05	1.25	24
7.....	1–30	PL + line + AD	58.5 ± 0.9	1.67	0.26 ± 0.14	6.1 ± 0.3	...	0.43 ± 0.07	1.27	24
Spectral File S32 (Maximum Intensity)										
1.....	3–30	PL	65.3 ± 2.8	1.70 ± 0.03	...	...	...	...	1.90	24
2.....	3–30	PL + line	66.6 ± 3.0	1.72 ± 0.03	0.36 ± 0.13	6.5 ± 0.2	...	...	1.20	22
3.....	1–30	PL	76.9 ± 2.0	1.79 ± 0.02	...	...	...	...	4.20	27
4.....	1–30	PL + line	78.7 ± 2.2	1.82 ± 0.02	0.41 ± 0.13	6.6 ± 0.2	...	...	3.50	25
5.....	1–30	PL + PL + line	65.3 ± 1.4	1.72	0.41 ± 0.14	6.5 ± 0.2	4.6 ± 0.80	...	1.40	24
6.....	1–30	PL + line + BB	66.0 ± 0.9	1.72	0.40 ± 0.13	6.5 ± 0.2	...	0.32 ± 0.05	1.10	24
7.....	1–30	PL + line + AD	65.9 ± 1.0	1.72	0.40 ± 0.13	6.5 ± 0.2	...	0.40 ± 0.07	1.10	24
B. 1988 Oct 12–13: *Ginga* LAC Observations										
Spectral File S4										
1.....	3–30	PL	50.2 ± 2.7	1.60 ± 0.03	...	...	...	...	1.90	24
2.....	3–30	PL + line	50.0 ± 2.7	1.60 ± 0.03	<0.016	<6.6	...	...	2.00	22
3.....	1–30	PL	55.2 ± 1.9	1.66 ± 0.02	...	...	...	...	2.40	27
4.....	1–30	PL + line	55.2 ± 2.0	1.66 ± 0.02	<0.012	<7.2	...	...	2.60	25
5.....	1–30	PL + PL	49.3 ± 1.0	1.60	...	...	4.70 ± 1.5	...	1.80	26
6.....	1–30	PL + BB	49.6 ± 0.7	1.60	...	...	...	0.30 ± 0.08	1.75	26
7.....	1–30	PL + AD	49.6 ± 0.7	1.60	...	...	...	0.37 ± 0.12	1.75	26
Spectral File S5										
1.....	3–30	PL	46.4 ± 1.9	1.63 ± 0.02	...	...	...	...	1.64	24
2.....	3–30	PL + line	46.9 ± 2.0	1.64 ± 0.02	0.20 ± 0.10	6.3 ± 0.3	...	...	1.33	22
3.....	1–30	PL	52.5 ± 1.4	1.70 ± 0.02	...	...	...	...	2.96	27
4.....	1–30	PL + line	53.1 ± 1.4	1.71 ± 0.02	0.21 ± 0.10	6.4 ± 0.3	...	...	2.74	25
5.....	1–30	PL + PL + line	46.0 ± 0.9	1.64	0.24 ± 0.11	6.3 ± 0.3	4.30 ± 1.	...	1.30	24
6.....	1–30	PL + line + BB	46.2 ± 0.7	1.64	0.25 ± 0.11	6.3 ± 0.3	...	0.36 ± 0.06	1.11	24
7.....	1–30	PL + line + AD	46.2 ± 0.7	1.64	0.25 ± 0.11	6.3 ± 0.3	...	0.46 ± 0.10	1.12	24

[a] In units of keV.

[b] PL: power law; BB: blackbody; AD: accretion disk; Line: Gaussian (width = 50 eV); $N_H = 4 \times 10^{20}$ cm^{-2} fixed from 21 cm measurements; quoted error bars are 90%.

[c] Normalization constants in units of photons s^{-1} keV^{-1}.

[d] χ_r^2 per degree of freedom, and DOF is the number of degrees of freedom.

TABLE 4

X-RAY FLUX[a] MEASURED FROM MRK 509

DATE OF OBSERVATION	TIME OF OBSERVATION[b]	ENERGY BAND (keV)					
		EXOSAT		*Ginga*			
		0.1–1	1–10	1–3	3–10	10–30	EW[c]
1988 Oct 8	0–2.3	...	...	3.0	4.2	5.8	109 ± 90
	3–4.9	...	...	3.5	4.8	6.1	79 ± 70
	6.1–9.5	...	...	3.75	5.1	6.6	87 ± 48
	9.5–14.2	...	...	4.0	5.3	6.5	150 ± 49
1988 Oct 12/13	20.8–3.4	...	...	3.1	4.8	6.9	[d]
1988 Oct 13	3.8–10.6	...	...	2.8	4.2	5.7	109 ± 44
1983 Oct 10	14.2–18.9	2.3	5.2	...	...	...	...
1983 Oct 22	11.9–15.0	3.8	6.0	...	...	...	...
1983 Nov 3	6.9–12.2	2.4	6.9	...	...	...	...

[a] In units of 10^{-11} ergs cm^{-2} s^{-1}.
[b] Start and end in hours (UT).
[c] Equivalent width of the line in eV.
[d] Line feature not required from χ^2 value.

χ^2. The hardening of the spectrum as the intensity decreases is also seen in this figure.

d) The Hardening of the X-Ray Spectrum at High Energies

We have also analyzed the X-ray spectra to look for any hardening at the high energies. For this purpose we divided the spectral data from 3 to 30 keV into two parts, 3–10 keV and 10–30 keV, and performed the spectral modeling separately on the two parts. To improve the efficiency for the 10–30 keV energy range, we summed the PH data from both the top and the middle layers of the LAC which have equal efficiency in this energy range. The data corresponding to the same intensity of the source were also added to improve the signal-to-noise ratio. We detect the presence of a hard component with $\Gamma = 1.47 \pm 0.07$ (90% error) in the 10–30 keV data with the highest signal to noise ratio (spectral files S31 and S32 summed) at the brightest phase of the source. In Figure 8 we show the 99% confidence contours obtained from the best-fit models to the 3–10 keV and the 10–30 keV PH data. The 3–10 keV PH data were fitted with a power law and a Gaussian, whereas the 10–30 keV data were fitted with a power law alone. The best-fit parameters and the χ^2 values are listed in Table 5. The significance of the detection of the hard component is quite evident from this figure where even the 99% confidence contours for the allowed range of the power-law indices from the two data sets have no overlap. That the observed hardening for energies greater than 10 keV is not an artifact of a poor background subtraction has been verified by looking at the data from the charge particle monitor and from the SUD (surplus over the upper discriminator) counter. These monitors showed that in the data analyzed, sudden increases which could have lead to poor modeling of the background were not present; instead, a slow decrease was noticed. The data at the lower intensity states, however, fail to show any evidence for the spectral hardening for energies greater than 10 keV (see Table 5).

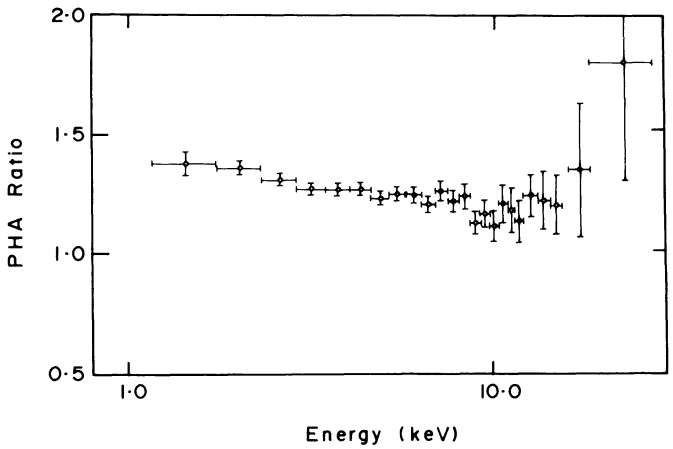

FIG. 7.—The plot of the PHA ratio, i.e., the ratio of the counts in each energy channel of the PHA at the brightest observed state (on October 8 from 06:00 UT to 14:15 UT) to the faintest observed state (on October 13 from 03:45 UT to 10:35 UT and on October 8 from 00:00 UT to 02:17 UT).

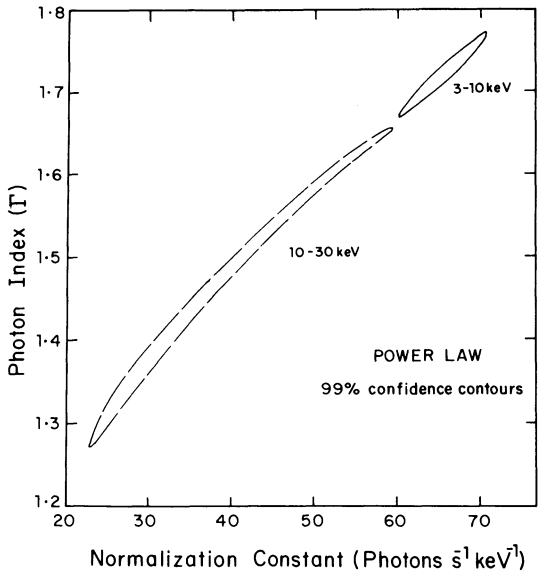

FIG. 8.—The 99% contours for the best-fit power-law index from the 3–10 keV spectral data and the 10–30 keV spectral data obtained on 1988 October 8 during the brightest phase of the source. The 3–10 keV data are from the top layer alone whereas the 10–30 keV spectrum was from the sum of the top and the middle layers of the LAC.

TABLE 5

RESULTS OF MODEL FITTING TO THE X-RAY SPECTRA[a] OF MRK 509

Serial Number	Energy Range[b]	Model[c]	A_1[d]	Γ	A_L[d]	E_L[b]	χ_r^2	DOF[e]
			Spectral File S31 + S32					
1.....	3–10	PL + line	65.3 ± 1.8	1.72 ± 0.02	0.31 ± 0.12	6.3 ± 0.22	0.92	7
2.....	10–30	PL	37.0 ± 6.8	1.47 ± 0.07	...	...	1.36	12
			Spectral File S1 + S5					
1.....	3–10	PL + line	49.2 ± 1.5	1.67 ± 0.02	0.23 ± 0.10	6.3 ± 0.25	2.6	7
2.....	10–30	PL	43.3 ± 7.9	1.60 ± 007	...	...	1.59	12
			Spectral File S2 + S4					
1.....	3–10	PL + line	57.0 ± 2.1	1.69 ± 0.02	0.19 ± 0.14	6.1 ± 0.40	0.81	7
2.....	10–30	PL	54.5 ± 14.	1.64 ± 0.10	...	...	0.63	12

[a] The 10–30 keV data is a sum of the top and the mid layers of the LAC.
[b] In units of keV.
[c] PL: power law; Line: a Gaussian.
[d] In units of photons s^{-1} keV^{-1}.
[e] Degrees of freedom.

IV. DISCUSSION

a) Short-Term Variability

It is generally believed that the universally observed variability in the active galactic nuclei (AGNs) is due to the release of the gravitational energy from the matter accreting onto a supermassive black hole thought to be existing in these AGNs. The energy is expected to be released from within a few times the Schwarzschild radius. The observed time variability can provide constraints on the apparent efficiency of the conversion of the rest mass to radiation and the black hole mass (see Fabian 1979). We have used the method suggested by Schwartz (1987) to quantify the observed variability and derive the constraints for the central source. We use the channel 2 count rates for this derivation. We have seen that the data for 1988 October 8 are well described by a quadratic expression (Table 2; Fig. 1). Assuming this behavior to be real and using the best-fit parameters, these data imply a slowly decreasing rate of change of luminosity. If the mass involved in the conversion of the rest mass energy into radiation is assumed to be constant, then a slowly decreasing efficiency of conversion can be inferred (or vice versa). It is also possible that the luminosity variation is a complex function of the two. Under the assumption of a constant accretion rate, the maximum efficiency would be given by

$$\eta_{\max} = 0.5 \times B \times l_{42} ,$$

where B is the value of the linear coefficient from Table 2 ($=3 \times 10^{-4}$), and l_{42} is the luminosity corresponding to a 1 LAC count s^{-1} in units of 10^{42} ergs s^{-1}. Using the value of 50 km s^{-1} Mpc^{-1} for the Hubble constant, we derive $\eta_{\max} =$ 0.0027. Following the minimum variability formalism of Schwartz (1987), the variability time scale (t_v) obtainable from the same data is given by $d/dt(f/\dot{f}) = 0$, where f is the best-fit quadratic expression. This implies that $t_v = 9 \times 10^4$ s ($\simeq$25 hr). From the light crossing time arguments, one would then obtain a radius of 2.7×10^{15} cm for the source. Assuming then that the radiation is coming from a Schwarzschild radius implies a black hole mass of 9×10^9 $M_\odot$. Similarly the data for 1988 October 12–13 imply a constant rate of change of luminosity and, under the same assumptions as above, an efficiency η of 0.0008. Using the maximum observed luminosity in the 1–30 keV energy band corresponding to the intensity of 1.6×10^{-10} ergs cm^{-2} s^{-1} and requiring this to be lower than the Eddington luminosity necessitates that the black hole mass be greater than 8.5×10^6 $M_\odot$. An efficiency of 0.0027 means that the accretion rate required to power this source is ~ 5.4 $M_\odot$ yr^{-1}.

b) Spectral Features Observed with Ginga and Their Comparison with the EXOSAT Observations

In Figure 9 we have plotted the spectral energy density as a function of the energy showing all the features detected with *Ginga*, viz., the steep low-energy component, the 3–10 keV continuum, the line feature near 6 keV, and the 10–30 keV hard component. The figure is based on the best fits to the data obtained when the source was at its brightest and thereby had the highest signal-to-noise ratio. We observe the following:

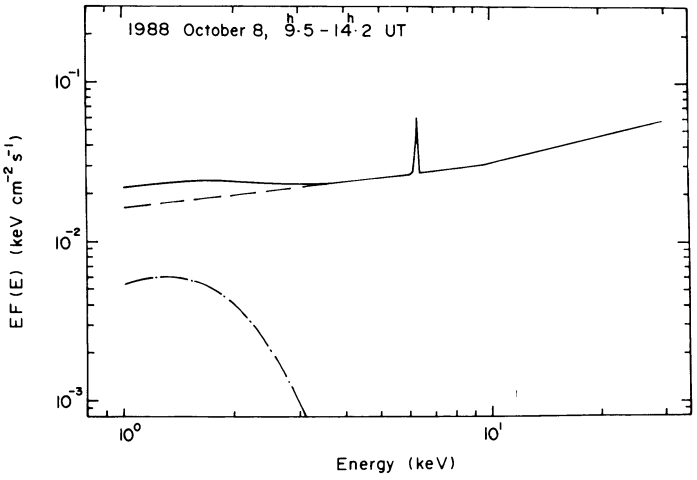

FIG. 9.—The energy spectrum of Mrk 509 observed with *Ginga* when the source was at its peak brightness. The diagram is an equivalent of the vF_v diagrams normally used to bring out subtle changes of the slope of the continua from the AGNs. The dashed curve shows the power-law component, the dotted-dashed curve shows the blackbody component at low energies, and the solid line shows the overall observed spectrum flattening out at energies greater than 10 keV and includes the line feature near 6 keV.

1. The steep low-energy excess seen with *Ginga* extends to higher energies than observed previously with either *HEAO 1* or *EXOSAT* (Singh, Garmire, and Nousek 1985 and Singh *et al.* 1989).

2. The 3–10 keV continuum follows the canonical power-law spectrum of the AGNs and is thus flatter than the 1–10 keV continuum observed with *EXOSAT* (Singh *et al.* 1989). There is also some evidence for a positive correlation between Γ and I_x.

3. The 6 keV line feature is much weaker than that reported by Morini, Lipani, and Molteni (1987) but consistent with its nondetection in the reanalysis of the *EXOSAT* data (Singh *et al.* 1989). The source was weaker in 1983 than in 1988, and at low intensity during the 1988 observations, the line feature was difficult to detect even with *Ginga*.

4. A hardening of the X-ray spectrum is observed for energies greater than 10 keV, when the source was in the brightest phase.

The extension of the low energy excess out to energies as high as 3 keV, observed with *Ginga* has also been reported from the combined analysis of the simultaneous SSS and the MPC observations with the *Einstein Observatory* (Holt *et al.* 1989). This fact could also be responsible for the observation of the steeper spectrum with *EXOSAT* in the 1–10 keV band. *EXOSAT*, because of its relatively poorer sensitivity, fails to resolve the high energy tail of the low-energy excess detected with *Ginga*. *Ginga*, on the other hand, is not sensitive to the very soft excess below 1 keV. This can be observed from Figure 10 which shows the spectral energy density plots obtained from *EXOSAT* and *Ginga* observations. The long term (days to years) spectral and intensity variations are also depicted in this figure. The marginal evidence for the steepening of the 3–10 keV power-law spectrum with the intensity that is observed with *Ginga* is not seen in the *EXOSAT* data. Considering that the amount of steepening is very small, its nondetection with *EXOSAT* could be due to the poorer sensitivity of *EXOSAT*. A similar steepening has, however, been observed in other low-luminosity ($L_x < 3 \times 10^{43}$ ergs s^{-1}) Seyferts, e.g., NGC 4151 (Perola *et al.* 1986; Yaqoob and Warwick 1989), NGC 5548 (Branduardi-Raymont 1986), NGC 4051, and MCG −6-30-15 (Matsuoka *et al.* 1990). The only other emission line AGN with luminosity comparable to that of Mrk 509 and showing similar spectral behavior is 3C 120 (Halpern 1985). Both the non-thermal and the thermal models of the X-ray continuum emission can reproduce such a steepening (Yaqoob and Warwick 1989; Dermer 1988).

The present observations do indicate that a single power law is not always adequate to explain the spectrum of Mrk 509. The mean spectrum as discerned from the Figure 10 does show a gradual flattening of the spectral index with increasing energy as hypothesized by Schwartz and Tucker (1988) to explain the diffuse X-ray-background as arising from the contributions of the AGNs.

The energy of the line feature is not measured very precisely with the present observations. Its detection between 6.0 and 6.5 keV is consistent with its origin in a hot thin plasma or due to the fluorescence of the cold iron in the neighborhood of the AGN. No absorption feature is, however, observed between 7 and 8 keV. A 90% confidence limit on the depth of the absorption edge corresponds to a hydrogen column density of log $N_H = 21.8$. This is consistent with almost no detectable absorption at low energies in the *Ginga* experiment. The assumption that the observed line at 6 keV is due to the fluorescence of cold iron is quite attractive as it implies the presence of considerable amount of cold matter around the X-ray source thus providing a natural explanation for the hardening of the 10–30 keV spectrum (see Lightman and White 1988 and Guilbert and Rees 1988) as being due to the reprocessing of the nonthermal X-rays by absorption and scattering in cold matter. It should also be noted that a considerable amount of gas around the AGN is required because of the poor efficiency of conversion of mass to the gravitational energy as discussed in § IV*a*. The observed equivalent width (EW) of 100–150 eV for the line is much larger than the value expected even if a column density as large as 10^{22} were to surround the source uniformly (Inoue 1985). Only a slablike configuration near the source can reproduce such an EW (Inoue 1985). The observations thus suggest an optically thick accretion disk very close to the X-ray source and with the line of sight to the source being nearly normal to the disk to account for both the observed soft excess and the line emission. The fact that the flattening of the hard X-ray emission is detected at the same time that line emission is detected most significantly is also consistent with the reprocessing of X-ray emission in a disk. Higher sensitivity broad-band X-ray observations with instruments having better energy resolution are required for a better detection of the effects of the cold matter around the AGN in Mrk 509. Such observations would be possible with the XTE and SPECTRUM-X-GAMMA missions planned for launch in the early 1990's. Simultaneous observations in the soft X-rays (with *ROSAT*), UV, and optical would help us to understand the spectral shape of the "big bump."

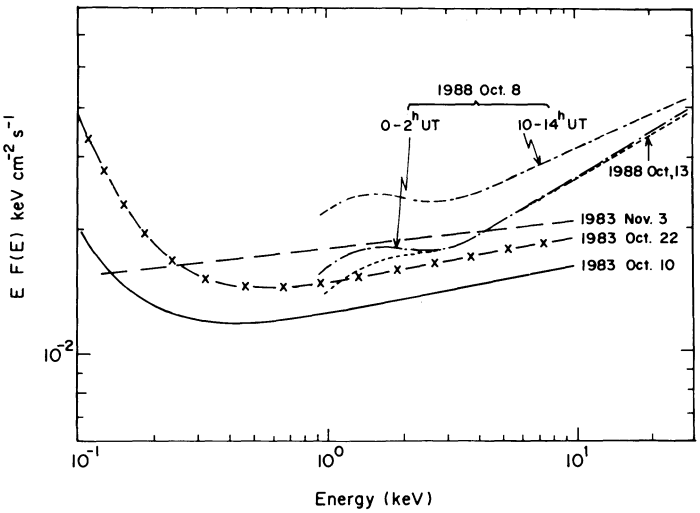

FIG. 10.—The energy spectra of Mrk 509 showing the time history of the spectral features observed with the *EXOSAT* and *Ginga*. The times at which the different spectra were obtained are marked in the figure. The *EXOSAT* measured spectra are shown for the 0.1–10 keV energy band, whereas those measured with *Ginga* are shown for the 1–30 keV band.

In a future publication, we would report on some of the simultaneous observations carried out at the radio (using the VLA), UV (using *IUE*), and optical wavelengths in conjunction with the X-ray observations reported here.

We would like to thank the *Ginga* Observatory team for carrying out the observations. One of us, K. P. S., would like to thank the Danish Space Research Institute for partial financial assistance toward the trip to Japan for carrying out the data reduction and analysis. We thank A. R. Rao for a critical reading of the manuscript.

REFERENCES

Antonucci, R., and Barvainis, R. 1988, *Ap. J. (Letters)*, **332**, L13.
Branduardi-Raymont, G. 1986, in *The Physics of Accretion onto Compact Objects*, ed. K. O. Mason, M. G. Watson, and N. E. White (Berlin: Springer-Verlag), p. 407.
Cooke, B. A., *et al.* 1978, *M.N.R.A.S.*, **182**, 489.
Dermer, C. D. 1988, *Ap. J. (Letters)*, **335**, L5.
Dil, S., *et al.* 1981, *Ap. J.*, **250**, 513.
Dower, R. G., Griffiths, R. E., Bradt, H. V., Doxsey, R. E., and Johnston, M. D. 1980, *Ap. J.*, **235**, 355.
Fabian, A. C. 1979, *Proc. Roy. Soc. London, A*, **366**, 449.
Guilbert, P., and Rees, M. J. 1988, *M.N.R.A.S.*, **233**, 475.
Halpern, J. P. 1985, *Ap. J.*, **290**, 130.
Hayashida, K., *et al.* 1989, *Pub. Astr. Soc. Japan*, **41**, 373.
Heiles, C. 1975, *Astr. Ap. Suppl.*, **20**, 37.
Holt, S. S., Turner, T. J., Mushotzky, R. F., and Weaver, K. 1989, in *Proc. of the 23rd ESLAB Symposium on Two Topics in X-ray Astronomy. II. AGN and the X-ray Background*, ed. J. Hunt and B. Battrick (ESA SP-296), p. 1105.
Inoue, H. 1985, in *Proc. Japan-US Seminar on Galactic and Extragalactic Compact X-ray Sources*, ed. Y. Tanaka and W. H. G. Lewin (Tokyo: ISAS), p. 153.
Kopylov, I. M., Lipovetskii, V. A., Pronik, V. I., and Chuvaev, K. K. 1974, *Astrofizika*, **10**, 483.
Lightman, A. P., and White, T. R. 1988, *Ap. J.*, **335**, 57.
Makino, F. 1987, *Ap. Letters Comm.*, **25**, 223.
Makishima, K., Maejima, Y., Mitsuda, K., Bradt, H. V., Remillard, R. A., Tuohy, I. R., Hoshi, R., and Nakagawa, M. 1986, *Ap. J.*, **308**, 635.
Matsuoka, M., Yamauchi, M., Piro, L., and Murakami, T. 1990, *Ap. J.*, in press.
Morini, M., Lipani, N. A., and Molteni, D. 1987, *Ap. J.*, **317**, 145.
Morrison, R., and McCammon, D. 1983, *Ap. J.*, **270**, 119.
Mushotzky, R. F., Marshall, R. E., Boldt, E. A., Holt, S. S., and Serlemitsos, P. J. 1980, *Ap. J.*, **235**, 377.
Perola, G. C., *et al.* 1986, *Ap. J.*, **306**, 508.
Petre, R., Mushotzky, R. F., Krolik, J. H., and Holt, S. S. 1984, *Ap. J.*, **280**, 499.
Philips, M. M., Baldwin, J. A., Atwood, B., and Carswell, R. F. 1983, *Ap. J.*, **274**, 558.
Rothschild, R., Mushotzky, R. F., Baity, W., Gruber, D., and Peterson, L. E. 1983, *Ap. J.*, **269**, 423.
Schwartz, D. A. 1987, *Ap. J.*, **318**, 568.
Schwartz, D. A., and Tucker, W. H. 1988, *Ap. J.*, **332**, 157.
Singh, K. P., Garmire, G. P., and Nousek, J. 1985, *Ap. J.*, **297**, 633.
Singh, K. P., Westergaard, N. J., Schnopper, H. W., Awaki, H. and Tawara, Y. 1989, in *Proc. of the 23rd ESLAB Symposium on Two Topics in X-ray Astronomy. II. AGN and the X-ray Background*, ed. J. Hunt and B. Battrick (ESA SP-296), p. 1053.
Turner, M. J. L., *et al.* 1989, *Pub. Astr. Soc. Japan*, **41**, 345.
Turner, T. J., and Pounds, K. A. 1989, *M.N.R.A.S.*, **240**, 833.
Ulvestad, J. S., and Wilson, A. S. 1984, *Ap. J.*, **278**, 544.
Warwick, R. S., Yaqoob, T., Pounds, K. A., Matsuoka, M., and Yamauchi, M. 1989, *Pub. Astr. Soc. Japan*, **41**, 721.
Wu, C. C., Boggess, J. A., and Gull, T. R. 1983, *Ap. J.*, **266**, 28.
Yaqoob, T., and Warwick, R. S. 1989, in *Proc. of the 23rd ESLAB Symposium on Two Topics in X-ray Astronomy. II. AGN and the X-ray Background*, ed. J. Hunt and B. Battrick (ESA SP-296), p. 1089.

H. AWAKI and Y. TAWARA: Department of Astrophysics, Nagoya University, Furo-cho, Chikusa-ku, Nagoya 464, Japan

H. W. SCHNOPPER and N. J. WESTERGAARD: Danish Space Research Institute, Lundtoftevej 7, 2800 Lyngby, Denmark

K. P. SINGH: X-Ray and Gamma-Ray Astronomy Group, Tata Institute of Fundamental Research, Homi Bhabha Road, Bombay-400 005, India